Investigating the specific role of external load on the performance versus stability trade-off in microbial fuel cells

László Koók, Nándor Nemestóthy, Katalin Bélafi-Bakó*, Péter Bakonyi

Research Institute on Bioengineering, Membrane Technology and Energetics, University of Pannonia, Egyetem u. 10, 8200 Veszprém, Hungary

*Corresponding Author: Prof. Katalin Bélafi-Bakó

Tel: +36 88 624726

E-mail: bako@almos.uni-pannon.hu

Abstract

The performance and behavior of microbial fuel cells (MFCs) are influenced by among others the external load (R_{ext}). In this study, the anode-surface biofilm formation in MFCs operated under different R_{ext} selection/tracking-strategies was assessed. MFCs were characterized by electrochemical (voltage/current generation, polarization tests, EIS), molecular biological (microbial consortium analysis) and bioinformatics (principal component analysis) tools. The results indicated that the MFC with dynamic R_{ext} adjustment (as a function of the actual MFC internal resistance) achieved notably higher performance but relatively lower operational stability, mainly due to the acidification of the biofilm. The opposite (lower performance, increased stability) could be observed with the static (low or high) R_{ext} application (or OCV) strategies, where adaptive microbial processes were assumed. These possible adaptation phenomena were outlined by a theoretical framework and the significant impact of R_{ext} on the anode colonization process and energy recovery with MFCs was concluded.

Keywords: microbial fuel cell; external load; current generation; biofilm formation; microbial community analysis; process stability

1. Introduction

The study of bioelectrochemical systems, such as microbial fuel cells (MFCs), requires a complex, multidisciplinary approach. The reason behind this is that the processes taking place in the MFCs are simultaneously related to material science, electrochemistry and microbiology (Bakonyi et al., 2018b; Patil et al., 2015). In fact, MFCs are electrochemical devices that, just like galvanic cells, can convert chemical energy directly into electric current (Logan et al., 2006; Pandey et al., 2016). Nevertheless, for the accomplishment of this task, MFCs applications rely on living microorganisms, in particular electrochemically active biocatalysts (EAB) (Kumar et al., 2015; Logan et al., 2019). In the MFCs, EABs begin to grow in colonies and form a biofilm on the surface of the anode electrode (provided that it is compatible with the microbes and their functioning) kept under anaerobic conditions (Logan et al., 2006). Furthermore, the substrate oxidation and electron transfer processes from the microbes to the anode (and further through the external circuit to the cathode) take also place here. The properties of this biofilm e.g. in terms of its electrochemical activity and quality (diversity) of EABs strongly determine the efficacy of the MFC (Bakonyi et al., 2018a; Koók et al., 2019b, 2018).

The efficiency of fuel cells such as MFCs, can be characterized by whole-cell polarization measurements, where the cell voltage is plotted against the generated current (density) at a given external resistance (R_{ext}) in order to obtain the maximum power (density) and the total internal resistance (R_{int}) of the fuel cell (Logan et al., 2006). However, the value of R_{int} - especially during the start-up phase of the MFC - may show notable temporal variability e.g. due to the development / maturation processes of the anode surface biofilm. In MFCs, the R_{int} is affected by three terms, such as activation/charge transfer, Ohmic (electrolyte) and concentration (diffusion, mass transfer) losses (Zhang and Liu, 2010). The operation of the MFCs should be maintained to generate maximum power density, which is theoretically expected at the point where $R_{ext} = R_{int}$ (Cell Design Point, CDP) (Raghavulu et al., 2009). Thus, a real-time optimization is suggested so that MFCs are kept at or close to CDP based on R_{int}-tracking strategy (Pinto et al., 2011). In order to real-time control R_{ext}, periodic disconnection of R_{ext} is needed, followed by the determination of the open circuit potential (OCV) of the MFC and voltage generation profile at various R_{ext} values (Pinto et al., 2011). Afterwards, the data are processed to display the current, power

as well as their relationship. Finally, a given maximum power-point tracking (MPPT) – usually perturbation observation (P/O) – algorithm can be used for choosing the optimal R_{ext} based on the change in the power (observation) to a set of R_{ext} (perturbation) (Pinto et al., 2011; Woodward et al., 2010). Interestingly, some studies demonstrated efficient MFC operation after an adaption to high currents applying low R_{ext} (Hong et al., 2011) or employing higher R_{ext} (Suzuki et al., 2018). On the whole, the importance and marked influence of R_{ext} on the anodic bioprocess using MFC seem to be confirmed (Katuri et al., 2011; Lyon et al., 2010; Pasternak et al., 2018; Rismani-Yazdi et al., 2011; Zhang et al., 2011). To have a deeper understanding of the process stability of MFCs operated under different external load conditions, it is clear that investigations in MFCs regarding the effect of time-dependent variation of R_{int}/R_{ext} and responses induced in the community of EAB on the anode surface, as well as their relationship to the MFC performance and stability are needed.

In the present study, therefore, the performance and stability of MFCs, as well as the changes of electrochemically-active, anode-surface biofilms were addressed under dynamic (adjusted to actual R_{int}) and static (fixed for the entire operation regardless of R_{int}) R_{ext} operating strategies employing electrochemical and molecular biological methods. In the former case, full cell polarization, cyclic voltammetry (CV) and electrochemical impedance spectroscopy (EIS) were undertaken, while useful, supporting information was extracted by microbial consortium analysis based on DNA-sequencing and metagenomics. By combining all of these data, the more detailed understanding of relationships between biotic and abiotic features of MFCs was put forward as the main objective. To enrich the literature in this specific field of bioelectrochemical systems, the comprehensive evaluation of experimental results was complemented by elaborating potential mechanisms for the various application scenarios of R_{ext}.

2. Materials and Methods

2.1. MFC setup and operation

The two-chambered MFCs were designed and operated as detailed previously (Koók et al., 2019a, 2019b). In brief, the MFCs were equipped with carbon felt anodes (Zoltek PX35, Zoltek Corp., USA) with apparent surface area of 30 cm^2, while the cathode electrode was made of Pt/carbon paper (0.3 mg Pt cm^{-2}, FuelCellsEtc, USA) (8 cm^2 apparent surface area). Ti wiring was used in the external electric circuit (Sigma-Aldrich, USA) between the electrodes. In order to investigate the effect of the external resistance (R_{ext}) applied, MFC external circuits were completed with either no resistor (open circuit mode, OCV-MFC), R_{ext} = 10 Ω (low resistance, Low-MFC), 10 kΩ (High resistance, High-MFC), or an external resistor dynamically changed according to the internal resistance (R_{int}) (Dyn-MFC).

The cathode chambers were filled with (160 mL) 50 mM, pH = 7.2 phosphate buffer solution (PBS). The anode chamber (160 mL) contained a mixture of activated anaerobic sludge collected from a municipal wastewater treatment plant (10 V/V %) and phosphate buffer, respectively. The initial pH of the anolyte was adjusted to 7.2, and acetate as a sole substrate was injected in batch mode during the experiments in 5 mM concentration. The anode and cathode compartments were separated using a Nafion 115 proton exchange membrane, which was pretreated as previously described (Ghasemi et al., 2013). The reactors were kept at a constant temperature of 37 °C.

2.2. Performance evaluation of MFCs

MFC voltage (V) was monitored and recorded by using a data logger, and the performance of the systems was evaluated by using the output indicators including the electric current (I) and power (P) (calculated according to Ohm's law regarding the voltage and the external resistance value, R_{ext}), as well as their anode-surface (A_a) standardized values, such as the current- and power densities (j and P_d, Eqs. 1 and 2) respectively.

$$j(t) = \frac{V(t)}{R_{ext} \cdot A_a} = \frac{I(t)}{A_a} \quad (1)$$

$$P_d(t) = \frac{V(t)^2}{R_{ext} \cdot A_a} = \frac{P(t)}{A_a} \quad (2)$$

Besides that, the energy recovery efficiency (η_E) and electron recovery efficiency (CE^*) were considered for the assessment of MFC behaviors according to Eqs. 3 and 4, respectively (Logan et al., 2006).

$$\eta_E = \frac{\int_0^\tau P(t) \cdot dt}{n_{Ac} \cdot \Delta H_{Ac}} \cdot 100\% \quad (3)$$

$$CE^* = \frac{M \cdot \int_0^\tau I(t) \cdot dt}{F \cdot b \cdot \Delta COD_{Ac} \cdot V_A} \cdot 100\% \quad (4)$$

As can be noted, η_E reflects the efficiency of gaining energy (kJ) from a certain quantity (n_{Ac}) of acetate loaded to the MFCs, considering its heat of combustion (ΔH_{Ac}). CE^* delivers the efficiency of cumulative electron utilization as charge compared to the charge theoretically obtainable from the organic matter (acetate) COD content (ΔCOD_{AC}). *M, F, b* and V_A stand for the molecular weight of oxygen gas, the Faraday's constant, the number of electrons per oxygen molecule and the volume of the anolyte, respectively.

2.3. Polarization tests

The MFC polarization tests were carried out by varying the external resistor in the electric circuit in the range of 10 kΩ - 10 Ω (20 min at each external resistor). Before recording the polarization curves, the external resistor (if any) was disconnected from the circuit for at least two hours to ensure OCV operation in advance to the tests. All measurements were done in the maximal current generation state (peak current) of the MFCs. The internal resistance of the MFCs at various operation stage was then determined from the slope of the Ohmic (linear) range of the registered voltage – current curves.

2.4. Cyclic voltammetry (CV)

In order to characterize the bioelectrochemical activity of MFC anode biofilms, cyclic Voltammetry (CV) measurements were carried out. CVs were recorded under non-turnover (substrate depleted) conditions using a PalmSens 3 potentiostat (PalmSens, Netherlands) and the data processing was done with PsTrace 5 software (PalmSens, Netherlands). The measurements were conducted in three-electrode configuration where an Ag/AgCl (3 M KCl) was employed as the reference electrode and the anode and cathode played the role of working and counter electrodes, respectively. The scan rate was set at 1 mV s^{-1} and an anode potential window of (+)0.25 V to (-)0.65 V was scanned.

2.5. Electrochemical Impedance Spectroscopy (EIS)

The decomposition of the total R_{int} to its components was carried out by using electrochemical impedance spectroscopy (EIS) and a PalmSens 3 potentiostat equipped with EIS feature (PalmSens, Netherlands). The measurement was done in two-electrode layout (whole-cell experimental setup) with the cathode as working and the anode as counter/reference electrodes, respectively. To conduct EIS, the frequency range of 50 kHz – 1 mHz was scanned with an AC amplitude of 10 mV. The data were collected under peak current density conditions of MFCs. In advance to the measurements, the external resistor was disconnected from the electric circuit of the reactors for at least two hours. The EIS Spectrum Analyser program (ABC Chemistry) was exploited to fit the equivalent circuit model. Based on the whole-cell EIS spectra, the decomposition of internal resistance of the MFCs was carried out resulting in charge transfer (R_{ct}), ohmic membrane + solution (R_{Ohm}) and diffusion (R_D) resistance components (Nam et al., 2010; Rezaei et al., 2007).

2.6. Microbial community assessment and principal component analysis

The microbial community analysis and related metagenomics assessment of the anodic biofilm samples taken from the MFCs operated under different external load strategies were conducted by following the procedure detailed in our recent

article (Koók et al., 2019b). Before analysis, the data were resampled using 78,917 reads per sample (the lowest number of reads obtained). The principal component analysis (PCA) was performed on relative abundances of main bacterial orders identified in the anodic biofilms of different MFCs, using IBM SPSS Statistics 24 software. Bacterial orders with a relative abundance > 1% in at least one sample were considered for the analysis. Based on bacterial genera, Shannon (*H'*) and Simpson (λ) phylogenetic diversity indices were calculated according to Eqs. 5 and 6, respectively.

$$H' = -\sum_{i=1}^{R} p_i \cdot \ln(p_i) \quad (5)$$

$$\lambda = \sum_{i=1}^{R} p_i^2 \quad (6)$$

where *R* denotes the richness (total number of genera) in the sample and p_i is the relative abundance of the genus *i*.

3. Results and Discussion

3.1. Descriptive assessment of MFCs

3.1.1. Electricity generation

In the field of MFCs, the term 'steady-state' should be addressed carefully, as electrochemical and biological steady-states may occur at distinct spots on the time-scale (Menicucci et al., 2006). The steady state, as defined within the frame of systems theory, cannot be fully achieved in such bioelectrochemical system at microscopic level due to reasons such as quantitative and qualitative changes in the anodic biofilm, the ongoing fouling on the membrane/cathode surface. Nevertheless, macroscopic steady-state can be indicated by consistent operation of MFCs when (usually 3) repeated impulses of the same feeding return with comparable voltage-, current-, power-generation profiles, Coulombic and substrate removal efficiencies as well as energy yields (Carmona-Martínez et al., 2015; Hashemi and Samimi, 2012; Menicucci et al., 2006).

In **Figs. 1A-D**, the voltage progress curves over the 6 cycles of acetate addition are shown for the MFCs operated under various external loads and in open circuit mode (infinite external resistance, when there is no any flow of current from the anode to the cathode). In the first four days after the point of inoculation, a pre-acclimation period was ensured without the injection of acetate substrate and thus, the organic matter inherently contained in the wastewater seed source could be consumed. Thereafter, acetate supplementation was commenced consecutively (5 mM in the anolyte, arrows in **Figs. 1A-D**) and polarization measurements were undertaken at the maximal current generation state (discussed in details in Section 3.2). At the end of the first acetate batch in the Dyn-MFC, the external load was switched to 470 Ω from 680 Ω ('I.' in **Fig. 1A**). The 2^{nd} and 3^{rd} cycles resulted in voltage curves with peak values comparable to the 1^{st} feeding. As illustrated by 'II.' in **Fig. 1A**, the external load was further reduced to 150 Ω. In the Low-MFC, a moderate decrease could be observed at the third peak's maximal voltage (**Fig. 1B**), while for High-MFC's voltage values, a slight increase was registered (**Fig. 1C**). In general, the current density was considered to indicate the stabilization of MFCs, with the exception of the OCV-MFC where due to the lack of current flow, voltage must have been used for this purpose. Maximal current densities under steady-state (variation of discrete peaks was < 7 %) were 266.6 ± 1.7, 424.6 ± 21.5 and 23.3 ± 1.6 mA m^{-2} for the Dyn-MFC, Low-MFC and High-MFC, respectively. Under steady-state conditions, peak voltages of 734.6 ± 24.2 mV were measured in the OCV-MFC (**Fig. 1D**). In successive (4^{th} and onwards) acetate feedings, quasi-stationary operational features were demonstrated by the MFCs excluding Dyn-MFC, for which voltage peak values declined gradually (**Fig. 1A**). During the 3 last substrate additions, Dyn-MFC and Low-MFC could be characterized by similar mean current density values, 440.4 ± 180.6 mA m^{-2} and 435.6 ± 32.7 mA m^{-2}, respectively. However, in the final cycle, relatively high fluctuation was noticed in the Dyn-MFC and current density as low as 288.9 mA m^{-2} was documented (**Fig. 2A**). Therefore, it would appear that the Dyn-MFC started-up via dynamic, stepwise tracking of internal resistance was unable to maintain steady-state. In contrast, the other MFCs (Low-MFC, High-MFC and OCV-MFC) acclimated under constant (static) external load or open circuit mode strategies seemed to fulfill the criteria of steady-state operation throughout the cycles.

Although rather un-steady current generation tendency was achieved by the Dyn-MFC, this setup provided even an order of magnitude higher performance

compared to Low-MFC and High-MFC. Actually, according to **Fig. 2B**, the power densities during the last 3 acetate cycles were as follows: 184.4 – 37.6 mW m^{-2} (Dyn-MFC), 10.4 ± 1.5 mW m^{-2} (Low-MFC) and 11.3 ± 4.7 mW m^{-2} (High-MFC).

3.1.2. Polarization characteristics

Whole-cell polarization tests were carried out at different stages of the MFC operation. In **Fig. 3A** presenting the results for the 3rd acetate feeding cycle, it can be seen that the Dyn-MFC significantly outperformed the other MFCs with maximum (polarization) power density (P_d^*) of > 200 mW m^{-2} and current density (j^*) of ~ 800 mA m^{-2}. At the lowest applied external resistance, current density reached 1 A m^{-2}. In contrast, power and current densities of other MFCs were significantly lower. In fact, High- and Low-MFCs were able to produce maximal P_d^* of 87 mW m^{-2} ($j^* \approx$ 320 mA m^{-2}), while P_d^* was 68 mW m^{-2} ($j^* \approx$ 200 mA m^{-2}) for the OCV-MFC (**Fig. 3A**). Among the 4 different MFC setups, the Dyn-MFC exhibited the lowest internal resistance (R_{int} = 122 Ω) followed by High-MFC, Low-MFC and OCV-MFC (R_{int} = 228 Ω, 360 Ω and 458 Ω, respectively).

From the polarization curves drawn at the end of the experiments (6th cycle) (**Fig. 3B**), it is to deduce that still the Dyn-MFC produced the highest P_d^* (and j^*) values, although the maximal P_d^* value and related current density decreased to 173 mW m^{-2} at $j^* \approx$ 700 mA m^{-2}, respectively. Moreover, the power overshoot phenomenon was strikingly experienced at high current densities in this MFC, causing a typical backdrop of P_d^* and j^* at low resistances (**Fig. 3B**). Consequently, R_{int} of Dyn-MFC increased from 122 Ω to 445 Ω, while it remained rather unchanged in High- and Low-MFCs. Moreover, further significant decrease of R_{int} (458 Ω → 170 Ω) in the OCV-MFC was noticed. This observation might be explained by the limitation processes taking over in Dyn-MFC e.g. compared to the previously seen data of the 3rd cycle. In addition, the least attractive P_d^* (30 mW m^{-2} at 130 mA m^{-2}) was attained by the Low-MFC. The above maximal power density range (30 – 173 mW m^{-2}) observed in this study with two-chamber, batch-type MFCs using (i) mixed culture as inoculum, (ii) Nafion membrane as separator and (iii) acetate as substrate are in good agreement with literature data, where MFCs of similar biotic and architectural traits were able to generate 38 mW m^{-2} (Min et al., 2005), 43.6 mW m^{-2} (Tang et al., 2010), 65 mW m^{-2} and 173.3 mW m^{-2} (Oh and Logan, 2006).

3.1.3. Cyclic voltammetry (CV) analysis under non-turnover conditions

Non-turnover (substrate-depleted) cyclic voltammograms (**Fig. 3C**) were registered after the 6th cycle in order to evaluate the activity of the biofilms on the anode. In general, all MFC biofilms reflected redox activity (cathodic and anodic peaks) within the scanned potential window. Although the redox peaks appeared at similar formal potentials, Dyn-MFC followed by Low-MFC demonstrated the highest peak currents, implying the presumably higher coverage of the anode by electro-active redox compounds e.g. cytochromes. This assumption is strengthened by the derivative CV curves (**Fig. 3D**), according to which the Dyn- and Low-MFC had remarkably higher $dI \cdot dE^{-1}$ values relative to High- and OCV-MFCs (**Fig. 3D**) and refer to enhanced bioelectrochemical activity (Hong et al., 2011). These observations are in good agreement with the current density ranges of the individual MFCs. However, CV curves and their derivatives suggest differences in terms of the redox properties of the biofilms between the Dyn-MFC and Low-MFC, while the High- and OCV-MFCs could be a way more identical.

3.2. MFC efficiency in the light of energy and charge recoveries

The evaluation of MFCs in terms of energy and charge recovery efficiencies – and their mutual relationship – can contribute to the elaboration of external resistance effect. As can be seen in **Fig. 4** for particular experimental setups (acetate batches of High-MFC and the first three cycles of Dyn-MFC) along the dashed line, the higher CE^* was coupled with higher η_E. As could be seen previously (Section 3.1), electricity generation in Dyn-MFC was keep on decreasing during the 4th-6th acetate feeding cycles and this is well-reflected in the corresponding CE^* and η_E values (**Fig. 4**). As for the Low-MFC, although high CE^* results were documented, η_E in this case seemed to be completely limited throughout the operating period.

Actually, η_E vs. CE^* in **Fig. 4** shows a clear analogy with the common power curves (P_d^* vs. j^*) of two-chamber MFCs where the power overshoot occurs (see for instance Figure 1 in the work of Nien et al. (Nien et al., 2011) or Figure 3 in the paper of Watson and Logan (Watson and Logan, 2011)). The decrease of MFC efficiency is usually related to the insufficient activity of the anodic biofilm (Kim et al., 2017)

caused often by increasing diffusion-limitation (associated with the transport of substrate to cell, e^- from cell to the anode or H^+ from the electrode towards the cathode) (De Lichtervelde et al., 2019).

From the above, it is to conclude that adequate efficiency in the Dyn-MFC could not be maintained for long (the peak performance was shortly followed by a persistent decrease of both η_E vs. CE^*). Nonetheless, one can observe that the operation under either charge transfer- (High-MFC and OCV-MFC) or mass transfer-limited (Low-MFC) regimes resulted in more stable but less-efficient performance. This suggests that a certain trade-off (where stability and performance are compromised) could be beneficial for sustaining MFC in longer-terms. To further elucidate these aspects, the internal resistance components and the anodic microbial communities of the MFCs will be investigated (Sections 3.5 and 3.6). This approach may help to reveal the effect of varied R_{ext} in the light of R_{int} in MFCs and support the examination of microbiological response strategies to architectural modifications related to R_{ext}.

3.3. Electrode potentials, internal resistance components and pH alterations during MFC operation at different external loads

Some essential data for discussing the MFC behaviors are presented in **Table 1**. In fact, anode potentials in all MFCs were found insignificantly different in most acetate feeding cycles, however, some literature studies reported the dependence of E_a on R_{ext} (Katuri et al., 2011; Menicucci et al., 2006). The cathode potentials were also similar except for High-MFC until the 3rd cycle, after which the MFCs with low or no current generation (High-MFC and OCV-MFC, respectively) were characterized by somewhat higher E_c in comparison with Dyn- and Low-MFCs. This can be attributed to the finding that high current densities, by hindering the oxygen reduction reaction (ORR), may cause larger cathodic losses (diffusion limitation) (Liang et al., 2007; Zhang et al., 2011).

Breakdown analysis of internal resistance using EIS technique indicates in general that the diffusion resistance (R_D) was the most substantial component of R_{int}, while the contributions of R_{CT} and R_{Ohm} were considered less significant (**Table 1**). Supportive experiences are frequently communicated in the literature (for systems without physical mixing such as in this work) (Hutchinson et al., 2011; Nam et al.,

2010; Ter Heijne et al., 2011; Wang and Yin, 2019). Actually, R_D gradually decreased in all the MFCs except in Dyn-MFC during the experiments (Supplementary material). In case of Dyn-MFC, after an initial decrease of R_D (where the performance increased simultaneously), the increment of R_D from 102.6 Ω to nearly 400 Ω was noted. Actually, the increment of R_D in Dyn-MFC over time may point to the occurrence of adverse mass transport conditions in the anode chamber. This matches with the previous discussion of polarization curves (Section 3.2) and energy and electron recovery efficiencies (Section 3.4), where biofilm malfunctioning and diffusion limitation were implied. The mass transfer conditions could be distinguished in the MFCs producing higher current or low/no current, as more than 2-times higher R_D values were encountered for the former group (comprising of Dyn-MFC and Low-MFC) compared to the latter one encompassing OCV-MFC and High-MFC. This could be seen supportive to the results of CV measurements (Section 3.3), according to which the anode surfaces of Low-MFC and Dyn-MFC could have been better enriched in redox-active components and thus, covered by a thicker biofilm.

The analysis of the pH for samples taken from the anode environment at the end of the cycles strengthens the assumption that mass transport limitation took place the Dyn-MFC. While OCV-, High- and Low-MFCs produced a relatively static final pH (6.6 – 7.1), the anolyte of Dyn-MFC became more acidic likely due to the accumulation of H^+. In fact, pH = 6.0 and 5.5 were measured at the end of the 3rd and 6th cycles, respectively that may have influenced the bioelectrochemical activity of the anode-respiring biofilm compared to previous cycles (Yuan et al., 2011). To get more useful feedback concerning the anodic biofilm behavior, respective microbial population analysis was carried out and elaborated in the next section.

3.4. The relationship between electrochemical and microbial properties

3.4.1. Microbial consortia analysis

Assessment of microbial communities in the anodic biofilms can promote the more confident understanding of MFC development and operational behavior under different external loads. In this work, the anodic biofilm samples were evaluated based on the number of OTUs, plus the Shannon and Simpson diversity indices. The lowest richness (low number of OTUs) and low evenness were found for the biofilm

of Dyn-MFC (Supplementary material). This means that the anode could be colonized only by a few phyla to form the electro-active biofilm. Shannon indexes were significantly higher in case of the other MFCs, and relatively high diversity was presented by the Simpson indexes in case of OCV-MFC and High-MFC (pointing to the increased number of phyla in the respective anodic biofilms).

The results of PCA analysis, as bioinformatics tool, supported that the maturation of anodic biofilm in Dyn-MFC and Low-MFC was notably different at the level of bacterial orders (**Fig. 5A**). As a matter of fact, Dyn-MFC had strongly negative value on Dim1 axis and moderate positive value on Dim2 axis. This correlates with the high relative abundance of the order *Desulfuromonadales*, and the minor contribution of *Spirochaetales* and *Bulkholderiales*, among others (**Fig. 5B**). On the contrary, in case of Low-MFC, moderate to high negative values are observable on Dim1 and Dim2 axes, respectively, which coincides with the high relative abundance of orders particularly *Rhodospirillales* and *Desulfuromonadales*. Concerning High-MFC and OCV-MFC, similar microbial selection progresses (differing significantly from those in Dyn-MFC and Low-MFC) were assumed. Actually, high positive value on the Dim1 axis and low positive value on the Dim2 axis can be noticed for both systems thanks to the dominant bacterial orders such as *Burkholderiales*, *Desulfuromonadales*, *Acholeplasmatales*, *Bacteroidales* and *Rhodocyclales* (**Figs. 5A-B**). The various members of these bacterial orders were found in bioelectrochemical systems such as MFCs (Koch et al., 2018; Oh et al., 2010), and it is important to discuss the complexity of anodic biofilms at lower taxonomic levels, particularly based on genera. From relative abundances of genera in **Table 2**, a complex selection process in the MFCs can be supposed. First of all, it should be underlined that the Dyn-MFC enriched *Geobacter* (36.95 %) the most among all MFCs and in addition, *Castellaniella*, *Pandoraea*, *Treponema*, *Serpentinomonas*, *Candidatus Cloacimonas*, *Clostridium* and *Brevefilum* were identified in 4.87 – 3.14 %. Thus, in this particular MFC biofilm, *Geobacter* was the predominant genus. The relatively high abundance of *Geobacter* was observed in Low-MFC (28.67 %), however, *Azospirillum* could be ranked as the most abundant genus (31.86 %). Other genera were present only in < 3 %. Furthermore, it turned out that the biofilms of High-MFC and OCV-MFC, on qualitative grounds, underwent a similar selection progress. Unlike in Dyn-MFC and Low-MFC, *Geobacter* and *Hydrogenophaga* were quasi-proportionally observed together. Compared to High-

MFC, OCV-MFC demonstrated larger abundance of *Geobacter* (20.69 % vs. 15.05 %) and *Hydrogenophaga* (26.60 % vs. 17.98 %).

3.4.2. Dissecting the results of electrochemical and molecular biological assays

In line with the colonization of anode, the electro-active biofilm gets thicker and consequently, an inner, dead-core layer may develop (between the anode surface and the outer, active layer of microorganisms) through which the electron transfer still needs to take place (Sun et al., 2015). Thus, accessibility of the electrode might become spatially hampered for some electro-active microbes to transfer their electrons and under such conditions, the adaption of the microbial consortia can be supposed in order to sustain anode-respiration. From our results on the microbial consortia analysis, it is inferred that the acclimatization of electro-active populations was different in MFCs applying various external load strategy. In essence, similar genera (and relatively diverse biofilm composition) were found in High-MFC and OCV-MFC compared to the other, Dyn- and Low-MFCs. In High-MFC and OCV-MFC, the current density was low to zero due to high external load and the open circuit operation, respectively. As it was reported in previous studies pertain to the effect of external resistance on biomass yield in MFCs, that only small amount of biofilm could be obtained using high resistances, although it was compact in structure and contained mostly active cells in addition to a moderate extent of EPS (Zhang et al., 2011). Moreover, the reduced flow of electrons caused by high external resistance (or the absence of current in case of OCV-MFC) may depress the metabolic activity of electro-active bacteria such as *Geobacter*, as supported by the outcomes of this work. In structurally compact biofilms, however, the diffusion of protons can get easily limited, which could lead to the even complete inactivation of electro-active bacteria due to the accumulation of H^+ and occurrence of pH < 5 locally. As for *Geobacter,* its capability to oxidize acetate into CO_2 and H_2 (Eq. 7) in the presence of biological hydrogen scavengers was documented. The removal of H_2 maintains its partial pressure low enough in order for the reaction in Eq. 7 to proceed (Cord-Ruwisch et al., 1998).

$$CH_3COO^- + H^+ + 2\,H_2O \rightarrow 2\,CO_2 + 4\,H_2 \qquad (\Delta G^{o\prime} = +95\ \mathrm{kJ\ mol^{-1}}) \qquad (7)$$

According to the discussion in Section 3.6, the growth of *Hydrogenophaga* along with *Geobacter* was observed in the biofilms of High-MFC and OCV-MFC, implying that indirect interspecies electron transfer (IIET) via H_2 could have taken place (**Fig. 6A**). Such cooperation between *Geobacter* and hydrogen-utilizing microbes has been explained in previous literature studies (Cord-Ruwisch et al., 1998; Kimura and Okabe, 2013a). Moreover, it was also concluded that *Hydrogenophaga* can demonstrate exoelectrogenic features (Kimura and Okabe, 2013b) and the contribution of cooperative hydrogen-consuming strains to the net electron flow can be as high as 5-10 % (Cord-Ruwisch et al., 1998). Therefore, it can be presumed that in High-MFC and OCV-MFC, a compact biofilm could have formed with relatively lower metabolic activity (supported by CV measurements) and in these cases, acetate oxidation in *Geobacter* may have been aided by *Hydrogenophaga*. This mechanism could be viewed as a strategic response (alternative metabolic pathway) to hindered electron transfer conditions. Moreover, the stability of anodic pH values suggests that the consumption of protons produced by exoelectrogens (according to Eq. 7) contributed to the steady – although less energy-productive – operation.

Based on the microbial consortia analysis, in Low-MFC, the flow of electrons was not remarkably obstructed because of the low external load (10 Ω), and the higher current densities (associated with the sufficient metabolic activity) were concomitant to a probably higher yield of biofilm. In fact, it was previously demonstrated in the literature (Zhang et al., 2011) that sub-optimal resistances induced the maturation of thicker but looser biofilm structure with greater portion of extracellular polymeric substances (EPS). In such a situation, more advantageous diffusion of substrate and protons to/from the biofilm, lower biofilm conductivity (as the cells are relatively far from each other compared to a compact biofilm) and mass transfer limitation of charge carriers (within the thick and loose biofilm layer) are likely (Zhang et al., 2011). At the anode of Low-MFC, the predominance of *Azospirillum* (non-fermentative, nitrogen-fixing genus from *Rhodospirillaceae* family) in addition to the population of *Geobacter* was experienced. The *Azospirillum* was found previously at MFC anodes of previous literature, however, its function/role has not been well-detailed (Pepè Sciarria et al., 2019; Xiao et al., 2015). Nevertheless, it is known that *Azospirillum* is able to accomplish EET via the reduction of anthraquinone-2,7-disulphonic acid (AQDS) (Zhou et al., 2013). Additionally, it was presumed and investigated in earlier studies that members of this genus could be able to alter the

pH in its microenvironment (Alonso and Marzocca, 1991). Hence, in Low-MFC (where the current flow is not externally hindered) with a thick and loose biofilm (having significant EPS content as supposed), the higher resistance to the electron transfer within the biofilm matrix may take place and the enrichment of *Azospirillum* besides *Geobacter* could be provoked in order to simultaneously facilitate the MFC operation by mediated EET (**Fig. 6B**). Moreover, since higher currents mean higher quantities of protons, *Azospirillum* may take part in the pH-balancing (neutralization) of the anodic environment (the measured pH values also assume negligible pH-splitting), as indicated previously (Alonso and Marzocca, 1991).

In Dyn-MFC, in which the external load was set close to the theoretical optimum ($R_{ext} = R_{int}$), the current- and power generation seemed to be sufficient and well-balanced during the adaption (start-up) period (Section 3.1). These, taking also into consideration the outputs of microbial consortia analysis, enlighten the improvement of MFC performance through adequate (varying/dynamic) external resistance strategy that more selectively promotes *Geobacter* spp. in the anodic biofilm (presumed to be rich in active microbial cells). However, this low microbial diversity (with remarkable enrichment of *Geobacter* spp.) could have an adverse effect on the stability of the Dyn-MFC. Actually, once the internal resistance of Dyn-MFC increased (after 3rd cycle, most likely due to the accumulation of protons in anodic microenvironments), the performance of the system declined consistently. As *Geobacter* seemed to be the main and predominant genus in the biofilm, it is our assumption that the Dyn-MFC was unable to preserve sufficient microbial activity and thus, keep the MFC working in a stable way. Nonetheless, despite an operational instability, it should be recalled that Dyn-MFC achieved the highest current and power densities. In summary, it would appear that although optimal external load conditions are beneficial for the selection of *Geobacter* spp. and enhance the MFC performance, the low microbiological diversity of the biofilm may lead to the lack of ability in managing the metabolism-related limitations (e.g. accumulation of protons).

In this section, the results were attempted to be elucidated by setting-up a plausible theoretical framework or in other words, a hypothesis-driven explanation regarding the behavior of MFCs start-up with different external load strategies. To verify or discard these ideas and assumed mechanisms behind the observed effects, future research will have to be conducted. It is proposed to investigate (i) how the biofilm composition/structure of Dyn-MFC changes in longer-terms (to reveal slow

post-adaptation, if any), (ii) what pattern the performance of decline follows in Dyn-MFC over time and find out if a new steady-state can be reached, and (iii) what is the exact role of different microbes other than *Geobacter* spp. in the biofilm. The data and assumptions presented here may be initiative for reconsidering the relationship between performance and operational stability of MFCs from the viewpoint of external load conditions and related microbiological responses.

4. Conclusions

In this work, the effect of different external load strategies was studied in microbial fuel cells. The Dyn-MFC, although showed significantly higher performance compared to other MFCs, failed to keep sufficient operational stability. It was assumed that the marked dominance of *Geobacter* spp. in the anodic biofilm of Dyn-MFC could have an adverse impact on the MFC stability, likely due to severe H^+ accumulation in vicinity of the anode. Meanwhile, High-, OCV- and Low-MFCs seemed to be more adaptive to the charge and mass transfer limitations at microbial level thanks to the co-existence of either *Hydrogenophaga* or *Azospirillum* with *Geobacter*.

Acknowledgements

Péter Bakonyi acknowledges the János Bolyai Research Scholarship of the Hungarian Academy of Sciences for the support. The financial support of this work by Széchenyi 2020 under the project GINOP-2.3.2-15-2016-00016 is gratefully appreciated.

Appendix A. Supplementary data

E-supplementary data for this work can be found in e-version of this paper online.

References

1. Alonso, M.R., Marzocca, M.C., 1991. Autoregulation of PH by Azospirillum Spp., in: Nitrogen Fixation. Springer, Dordrecht, pp. 303–304. https://doi.org/10.1007/978-94-011-3486-6_57
2. Bakonyi, P., Koók, L., Keller, E., Bélafi-Bakó, K., Rózsenberszki, T., Saratale, G.D., Nguyen, D.D., Banu, J.R., Nemestóthy, N., 2018a. Development of bioelectrochemical systems using various biogas fermenter effluents as inocula and municipal waste liquor as adapting substrate. Bioresour. Technol. 259, 75–82. https://doi.org/10.1016/j.biortech.2018.03.034
3. Bakonyi, P., Koók, L., Kumar, G., Tóth, G., Rózsenberszki, T., Nguyen, D.D., Chang, S.W., Zhen, G., Bélafi-Bakó, K., Nemestóthy, N., 2018b. Architectural engineering of bioelectrochemical systems from the perspective of polymeric membrane separators: A comprehensive update on recent progress and future prospects. J. Membr. Sci. 564, 508–522. https://doi.org/10.1016/j.memsci.2018.07.051
4. Carmona-Martínez, A.A., Trably, E., Milferstedt, K., Lacroix, R., Etcheverry, L., Bernet, N., 2015. Long-term continuous production of H<inf>2</inf> in a microbial electrolysis cell (MEC) treating saline wastewater. Water Res. 81, 149–156. https://doi.org/10.1016/j.watres.2015.05.041
5. Cord-Ruwisch, R., Lovley, D.R., Schink, B., 1998. Growth of Geobacter sulfurreducens with acetate in syntrophic cooperation with hydrogen-oxidizing anaerobic partners. Appl. Environ. Microbiol. 64, 2232–2236.
6. De Lichtervelde, A.C.L., Ter Heijne, A., Hamelers, H.V.M., Biesheuvel, P.M., Dykstra, J.E., 2019. Theory of Ion and Electron Transport Coupled with Biochemical Conversions in an Electroactive Biofilm. Phys. Rev. Appl. 12. https://doi.org/10.1103/PhysRevApplied.12.014018
7. Ghasemi, M., Wan Daud, W.R., Ismail, M., Rahimnejad, M., Ismail, A.F., Leong, J.X., Miskan, M., Ben Liew, K., 2013. Effect of pre-treatment and biofouling of proton exchange membrane on microbial fuel cell performance. Int. J. Hydrogen Energ. 38, 5480–5484. https://doi.org/10.1016/j.ijhydene.2012.09.148
8. Hashemi, J., Samimi, A., 2012. Steady state electric power generation in up-flow microbial fuel cell using the estimated time span method for bacteria

591 growth domestic wastewater. Biomass Bioenerg. 45, 65–76.
592 https://doi.org/10.1016/j.biombioe.2012.05.011
593 9. Hong, Y., Call, D.F., Werner, C.M., Logan, B.E., 2011. Adaptation to high
594 current using low external resistances eliminates power overshoot in microbial
595 fuel cells. Biosens. Bioelectron. 28, 71–76.
596 https://doi.org/10.1016/j.bios.2011.06.045
597 10. Hutchinson, A.J., Tokash, J.C., Logan, B.E., 2011. Analysis of carbon fiber
598 brush loading in anodes on startup and performance of microbial fuel cells. J.
599 Power Sources 196, 9213–9219.
600 https://doi.org/10.1016/j.jpowsour.2011.07.040
601 11. Katuri, K.P., Scott, K., Head, I.M., Picioreanu, C., Curtis, T.P., 2011. Microbial
602 fuel cells meet with external resistance. Bioresour. Technol. 102, 2758–2766.
603 https://doi.org/10.1016/j.biortech.2010.10.147
604 12. Kim, B., An, J., Chang, I.S., 2017. Elimination of Power Overshoot at
605 Bioanode through Assistance Current in Microbial Fuel Cells. ChemSusChem
606 10, 612–617. https://doi.org/10.1002/cssc.201601412
607 13. Kimura, Z.I., Okabe, S., 2013a. Acetate oxidation by syntrophic association
608 between Geobacter sulfurreducens and a hydrogen-utilizing exoelectrogen.
609 ISME J. 7, 1472–1482. https://doi.org/10.1038/ismej.2013.40
610 14. Kimura, Z.I., Okabe, S., 2013b. Hydrogenophaga electricum sp. nov., isolated
611 from anodic biofilms of an acetate-fed microbial fuel cell. Journal of General
612 and Appl. Microbiol. 59, 261–266. https://doi.org/10.2323/jgam.59.261
613 15. Koch, C., Korth, B., Harnisch, F., 2018. Microbial ecology-based engineering
614 of Microbial Electrochemical Technologies. Microb. Biotechnol. 11, 22–38.
615 https://doi.org/10.1111/1751-7915.12802
616 16. Koók, L., Kanyó, N., Dévényi, F., Bakonyi, P., Rózsenberszki, T., Bélafi-Bakó,
617 K., Nemestóthy, N., 2018. Improvement of waste-fed bioelectrochemical
618 system performance by selected electro-active microbes: Process evaluation
619 and a kinetic study. Biochem. Eng. J. 137, 100–107.
620 https://doi.org/10.1016/j.bej.2018.05.020
621 17. Koók, L., Kaufer, B., Bakonyi, P., Rózsenberszki, T., Rivera, I., Buitrón, G.,
622 Bélafi-Bakó, K., Nemestóthy, N., 2019a. Supported ionic liquid membrane
623 based on [bmim][PF6] can be a promising separator to replace Nafion in
624 microbial fuel cells and improve energy recovery: A comparative process

625 evaluation. J. Membr. Sci. 570–571, 215–225.
626 https://doi.org/10.1016/j.memsci.2018.10.063
627 18. Koók, L., Quéméner, E.D. Le, Bakonyi, P., Zitka, J., Trably, E., Tóth, G.,
628 Pavlovec, L., Pientka, Z., Bernet, N., Bélafi-Bakó, K., Nemestóthy, N., 2019b.
629 Behavior of two-chamber microbial electrochemical systems started-up with
630 different ion-exchange membrane separators. Bioresour. Technol. 278, 279–
631 286. https://doi.org/10.1016/j.biortech.2019.01.097
632 19. Kumar, R., Singh, L., Wahid, Z.A., Din, M.F.M., 2015. Exoelectrogens in
633 microbial fuel cells toward bioelectricity generation: A review. Int. J. Energ.
634 Res. 39, 1048–1067. https://doi.org/10.1002/er.3305
635 20. Liang, P., Huang, X., Fan, M.Z., Cao, X.X., Wang, C., 2007. Composition and
636 distribution of internal resistance in three types of microbial fuel cells. Appl.
637 Microbiol. Biotechnol. 77, 551–558. https://doi.org/10.1007/s00253-007-1193-
638 4
639 21. Logan, B.E., Hamelers, B., Rozendal, R., Schröder, U., Keller, J., Freguia, S.,
640 Aelterman, P., Verstraete, W., Rabaey, K., 2006. Microbial fuel cells:
641 Methodology and technology. Environ. Sci. Technol. 40, 5181–5192.
642 https://doi.org/10.1021/es0605016
643 22. Logan, B.E., Rossi, R., Ragab, A., Saikaly, P.E., 2019. Electroactive
644 microorganisms in bioelectrochemical systems. Nat. Rev. Microbiol. 17, 307–
645 319. https://doi.org/10.1038/s41579-019-0173-x
646 23. Lyon, D.Y., Buret, F., Vogel, T.M., Monier, J.M., 2010. Is resistance futile?
647 Changing external resistance does not improve microbial fuel cell
648 performance. Bioelectrochemistry 78, 2–7.
649 https://doi.org/10.1016/j.bioelechem.2009.09.001
650 24. Menicucci, J., Beyenal, H., Marsili, E., Veluchamy, R.A., Demir, G.,
651 Lewandowski, Z., 2006. Procedure for determining maximum sustainable
652 power generated by microbial fuel cells. Environ. Sci. Technol. 40, 1062–1068.
653 https://doi.org/10.1021/es051180l
654 25. Min, B., Cheng, S., Logan, B.E., 2005. Electricity generation using membrane
655 and salt bridge microbial fuel cells. Water Res. 39, 1675–1686.
656 https://doi.org/10.1016/j.watres.2005.02.002
657 26. Nam, J.Y., Kim, H.W., Lim, K.H., Shin, H.S., Logan, B.E., 2010. Variation of
658 power generation at different buffer types and conductivities in single chamber

659 microbial fuel cells. Biosens. Bioelectron. 25, 1155–1159.
660 https://doi.org/10.1016/j.bios.2009.10.005
661 27. Nien, P.C., Lee, C.Y., Ho, K.C., Adav, S.S., Liu, L., Wang, A., Ren, N., Lee,
662 D.J., 2011. Power overshoot in two-chambered microbial fuel cell (MFC).
663 Bioresour. Technol. 102, 4742–4746.
664 https://doi.org/10.1016/j.biortech.2010.12.015
665 28. Oh, S.E., Logan, B.E., 2006. Proton exchange membrane and electrode
666 surface areas as factors that affect power generation in microbial fuel cells.
667 Appl. Microbiol. Biotechnol. 70, 162–169. https://doi.org/10.1007/s00253-005-
668 0066-y
669 29. Oh, S.T., Kim, J.R., Premier, G.C., Lee, T.H., Kim, C., Sloan, W.T., 2010.
670 Sustainable wastewater treatment: How might microbial fuel cells contribute.
671 Biotechnol. Adv. 28, 871–881.
672 https://doi.org/10.1016/j.biotechadv.2010.07.008
673 30. Pandey, P., Shinde, V.N., Deopurkar, R.L., Kale, S.P., Patil, S.A., Pant, D.,
674 2016. Recent advances in the use of different substrates in microbial fuel cells
675 toward wastewater treatment and simultaneous energy recovery. Appl. Energ.
676 168, 706–723. https://doi.org/10.1016/j.apenergy.2016.01.056
677 31. Pasternak, G., Greenman, J., Ieropoulos, I., 2018. Dynamic evolution of
678 anodic biofilm when maturing under different external resistive loads in
679 microbial fuel cells. Electrochemical perspective. J. Power Sources 400, 392–
680 401. https://doi.org/10.1016/j.jpowsour.2018.08.031
681 32. Patil, S.A., Gildemyn, S., Pant, D., Zengler, K., Logan, B.E., Rabaey, K., 2015.
682 A logical data representation framework for electricity-driven bioproduction
683 processes. Biotechnol. Adv. 33, 736–744.
684 https://doi.org/10.1016/j.biotechadv.2015.03.002
685 33. Pepè Sciarria, T., Arioli, S., Gargari, G., Mora, D., Adani, F., 2019. Monitoring
686 microbial communities' dynamics during the start-up of microbial fuel cells by
687 high-throughput screening techniques. Biotechnol. Rep. 21.
688 https://doi.org/10.1016/j.btre.2019.e00310
689 34. Pinto, R.P., Srinivasan, B., Uiot, S.R., Tartakovsky, B., 2011. The effect of
690 real-time external resistance optimization on microbial fuel cell performance.
691 Water Res. 45, 1571–1578. https://doi.org/10.1016/j.watres.2010.11.033
692 35. Raghavulu, S.V., Mohan, S.V., Goud, R.K., Sarma, P.N., 2009. Effect of

693 anodic pH microenvironment on microbial fuel cell (MFC) performance in
694 concurrence with aerated and ferricyanide catholytes. Electrochem. Commun.
695 11, 371–375. https://doi.org/10.1016/j.elecom.2008.11.038
696 36. Rezaei, F., Richard, T.L., Brennan, R.A., Logan, B.E., 2007. Substrate-
697 enhanced microbial fuel cells for improved remote power generation from
698 sediment-based systems. Environ. Sci. Technol. 41, 4053–4058.
699 https://doi.org/10.1021/es070426e
700 37. Rismani-Yazdi, H., Christy, A.D., Carver, S.M., Yu, Z., Dehority, B.A.,
701 Tuovinen, O.H., 2011. Effect of external resistance on bacterial diversity and
702 metabolism in cellulose-fed microbial fuel cells. Bioresour. Technol. 102, 278–
703 283. https://doi.org/10.1016/j.biortech.2010.05.012
704 38. Sun, D., Cheng, S., Wang, A., Li, F., Logan, B.E., Cen, K., 2015. Temporal-
705 spatial changes in viabilities and electrochemical properties of anode biofilms.
706 Environ. Sci. Technol. 49, 5227–5235.
707 https://doi.org/10.1021/acs.est.5b00175
708 39. Suzuki, K., Kato, Y., Yui, A., Yamamoto, S., Ando, S., Rubaba, O., Tashiro, Y.,
709 Futamata, H., 2018. Bacterial communities adapted to higher external
710 resistance can reduce the onset potential of anode in microbial fuel cells. J.
711 Biosci. Bioeng. 125, 565–571. https://doi.org/10.1016/j.jbiosc.2017.12.018
712 40. Tang, X., Guo, K., Li, H., Du, Z., Tian, J., 2010. Microfiltration membrane
713 performance in two-chamber microbial fuel cells. Biochem. Eng. J. 52, 194–
714 198. https://doi.org/10.1016/j.bej.2010.08.007
715 41. Ter Heijne, A., Schaetzle, O., Gimenez, S., Fabregat-Santiago, F., Bisquert,
716 J., Strik, D.P.B.T.B., Barrière, F., Buisman, C.J.N., Hamelers, H.V.M., 2011.
717 Identifying charge and mass transfer resistances of an oxygen reducing
718 biocathode. Energ. Environ. Sci. 4, 5035–5043.
719 https://doi.org/10.1039/c1ee02131a
720 42. Wang, J., Yin, Y., 2019. Progress in microbiology for fermentative hydrogen
721 production from organic wastes. Crit. Rev. Environ. Sci. Technol. 49, 825–865.
722 https://doi.org/10.1080/10643389.2018.1487226
723 43. Watson, V.J., Logan, B.E., 2011. Analysis of polarization methods for
724 elimination of power overshoot in microbial fuel cells. Electrochem. Commun.
725 13, 54–56. https://doi.org/10.1016/j.elecom.2010.11.011
726 44. Woodward, L., Perrier, M., Srinivasan, B., Pinto, R.P., Tartakovsky, B., 2010.

727 Comparison of real-time methods for maximizing power output in microbial fuel
728 cells. AIChE J. 56, 2742–2750. https://doi.org/10.1002/aic.12157
729 45. Xiao, Y., Zheng, Y., Wu, S., Zhang, E.H., Chen, Z., Liang, P., Huang, X.,
730 Yang, Z.H., Ng, I.S., Chen, B.Y., Zhao, F., 2015. Pyrosequencing reveals a
731 core community of anodic bacterial biofilms in bioelectrochemical systems
732 from China. Front. Microbiol. 6, 1410.
733 https://doi.org/10.3389/fmicb.2015.01410
734 46. Yuan, Y., Zhao, B., Zhou, S., Zhong, S., Zhuang, L., 2011. Electrocatalytic
735 activity of anodic biofilm responses to pH changes in microbial fuel cells.
736 Bioresour. Technol. 102, 6887–6891.
737 https://doi.org/10.1016/j.biortech.2011.04.008
738 47. Zhang, F., Merrill, M.D., Tokash, J.C., Saito, T., Cheng, S., Hickner, M.A.,
739 Logan, B.E., 2011. Mesh optimization for microbial fuel cell cathodes
740 constructed around stainless steel mesh current collectors. J. Power Sources
741 196, 1097–1102. https://doi.org/10.1016/j.jpowsour.2010.08.011
742 48. Zhang, L., Zhu, X., Li, J., Liao, Q., Ye, D., 2011. Biofilm formation and
743 electricity generation of a microbial fuel cell started up under different external
744 resistances. J. Power Sources 196, 6029–6035.
745 https://doi.org/10.1016/j.jpowsour.2011.04.013
746 49. Zhang, P.Y., Liu, Z.L., 2010. Experimental study of the microbial fuel cell
747 internal resistance. J. Power Sources 195, 8013–8018.
748 https://doi.org/10.1016/j.jpowsour.2010.06.062
749 50. Zhou, S., Han, L., Wang, Y., Yang, G., Li, Z., Hu, P., 2013. Azospirillum
750 humicireducens sp. nov., a nitrogen-fixing bacterium isolated from a microbial
751 fuel cell. Int. J. Syst. Evol. Micr. 63, 2618–2624.
752 https://doi.org/10.1099/ijs.0.046813-0
753

Figure captions

Fig. 1 – The voltage vs. time profiles of 5 mM acetate batches in MFCs operating under various external load strategy. (A): Dyn-MFC; (B): Low-MFC; (C): High-MFC; (D): OCV-MFC. Substrate additions are indicated by arrows.

Fig. 2 – Peak current density (A) and power density (B) values of the consecutive acetate cycles.

Fig. 3 – The results of polarization measurements of different MFCs. (A-B): power curves at the maximal current generating state of the 3^{rd} (A) and 6^{th} (B) acetate cycles; (C-D): non-turnover cyclic voltammogram (C) and its derivative (D) for the various MFCs subsequent to the 6^{th} acetate cycle.

Fig. 4 – The relationship between electron and energy recovery efficiencies of the different MFCs.

Fig. 5 – Results of principal component analysis (PCA) performed on relative abundances of main bacterial orders identified in the anodic biofilms of different MFCs. (A): Individual factor map showing the positions of anodic biofilm sample communities on the axes Dim1 and Dim2; (B): variable factor map representing the contributions of bacterial orders to Dim1 and Dim2. Only orders with a relative abundance > 1% in at least two samples were used for the analysis.

Fig. 6 – Hypothesized bacterial adaptation strategies to charge transfer (A) and mass transfer (B) limited operations considering the microbial consortia analysis. High- and OCV-MFCs presumably behaved according to the mechanism (A), while Low-MFC is assumed to follow mechanism (B). (C) shows the case of Dyn-MFC.

778 **Table 1** – Electrode potentials, internal resistance components and anodic pH values
779 of MFCs at different stages of operation.

780

		External load strategy			
	Cycle	**OCV-MFC**	**High-MFC**	**Dyn-MFC**	**Low-MFC**
OCV (V)	1st	0.678	0.567	0.725	0.691
	3rd	0.710	0.640	0.695	0.700
	6th	0.735	0.675	0.642	0.580
E_a (V)	1st	-0.285	-0.400	-0.404	-0.396
	3rd	-0.481	-0.492	-0.468	-0.472
	6th	-0.470	-0.430	-0.480	-0.425
E_c (V)	1st	0.393	0.167	0.321	0.295
	3rd	0.229	0.148	0.227	0.228
	6th	0.265	0.245	0.162	0.155
R_{int} (Ω)	1st	979	816	439	1412
	3rd	458	228	122	360
	6th	170	218	445	365
R_{Ohm} (Ω)	1st	22.0	24.6	17.6	23.7
	3rd	17.9	15.2	15.6	15.5
	6th	11.1	29.1	14.3	12.4
R_{CT} (Ω)	1st	6.8	1.5	0.9	6.5
	3rd	9.6	4.0	3.8	2.9
	6th	8.1	22.3	31.0	14.6
R_D (Ω)	1st	950.2	789.9	420.5	1381.8
	3rd	430.5	208.8	102.6	341.6
	6th	150.8	166.6	399.7	338.0
pH_{an} (-)	1st	6.8	7.0	6.7	7.1
	3rd	7.1	6.9	6.3	6.6
	6th	6.7	6.9	5.5	6.8

781 *All potential values are given against Ag/AgCl (3M KCl) reference electrode.

782 **Table 2** – Relative abundance of main genera found in anodic biofilms of different
783 MFCs.
784

	Relative abundance (%)			
Genera	**Dyn-MFC**	**Low-MFC**	**High-MFC**	**OCV-MFC**
Geobacter	36.95	28.67	15.05	20.69
Azospirillum	N.D.	31.86	N.D.	N.D.
Hydrogenophaga	2.50	2.88	17.98	26.60
Acholeplasma	N.D.	N.D.	8.54	4.81
Proteiniphilum	N.D.	N.D.	6.74	8.14
Azoarcus	N.D.	1.35	5.00	2.78
Castellaniella	4.87	N.D.	N.D.	N.D.
Pandoraea	4.62	N.D.	N.D.	N.D.
Treponema	4.09	1.89	1.63	N.D.
Serpentinomonas	3.77	N.D.	N.D.	N.D.
Candidatus Cloacimonas	3.48	1.21	1.98	N.D.
Petrimonas	N.D.	1.97	2.30	3.45
Clostridium	3.26	N.D.	N.D.	N.D.
Brevefilum	3.14	N.D.	1.06	1.21
Other	33.32	30.17	39.72	32.32

785 * N.D. – Not detected
786

Fig. 1

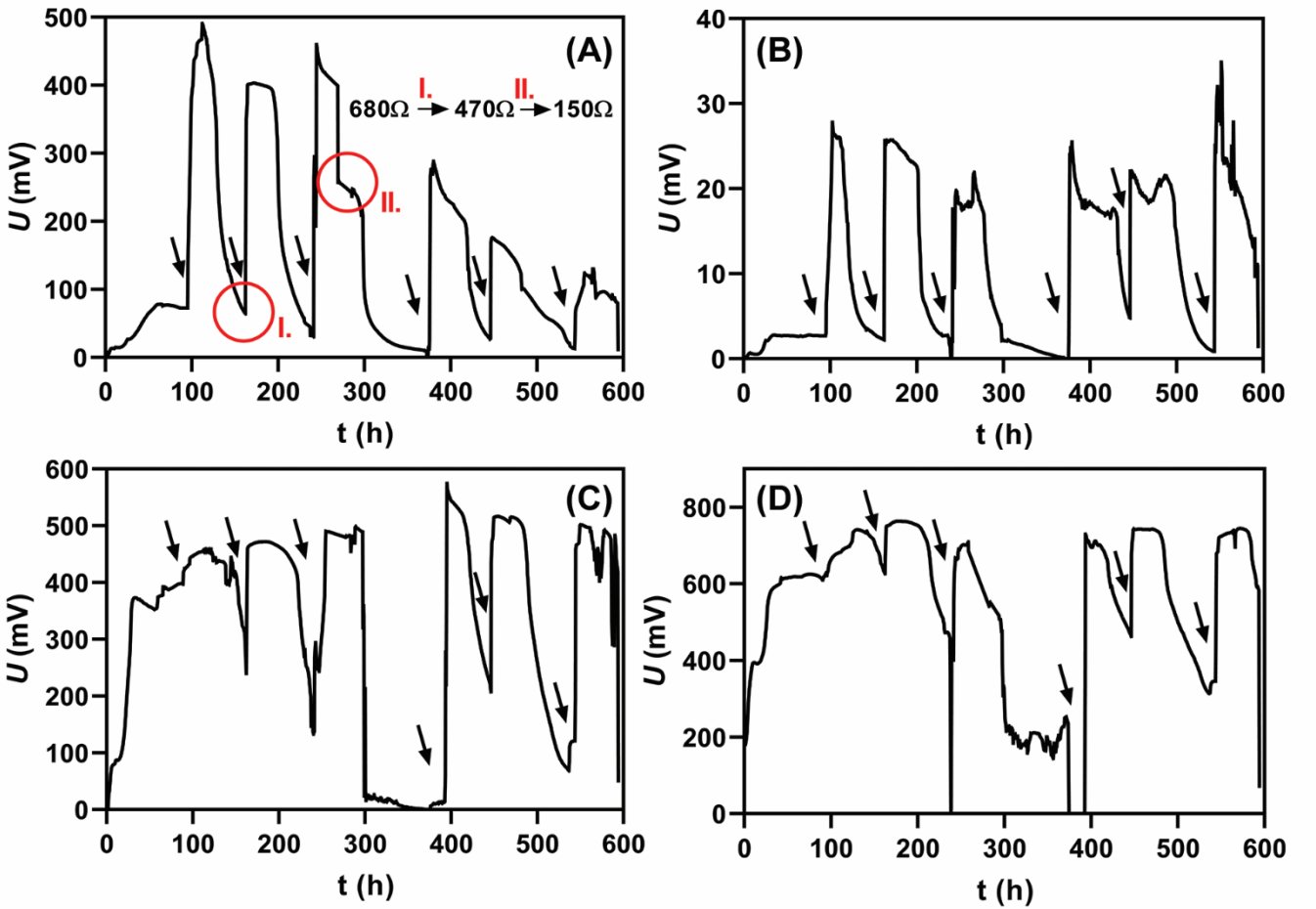

790 **Fig. 2**

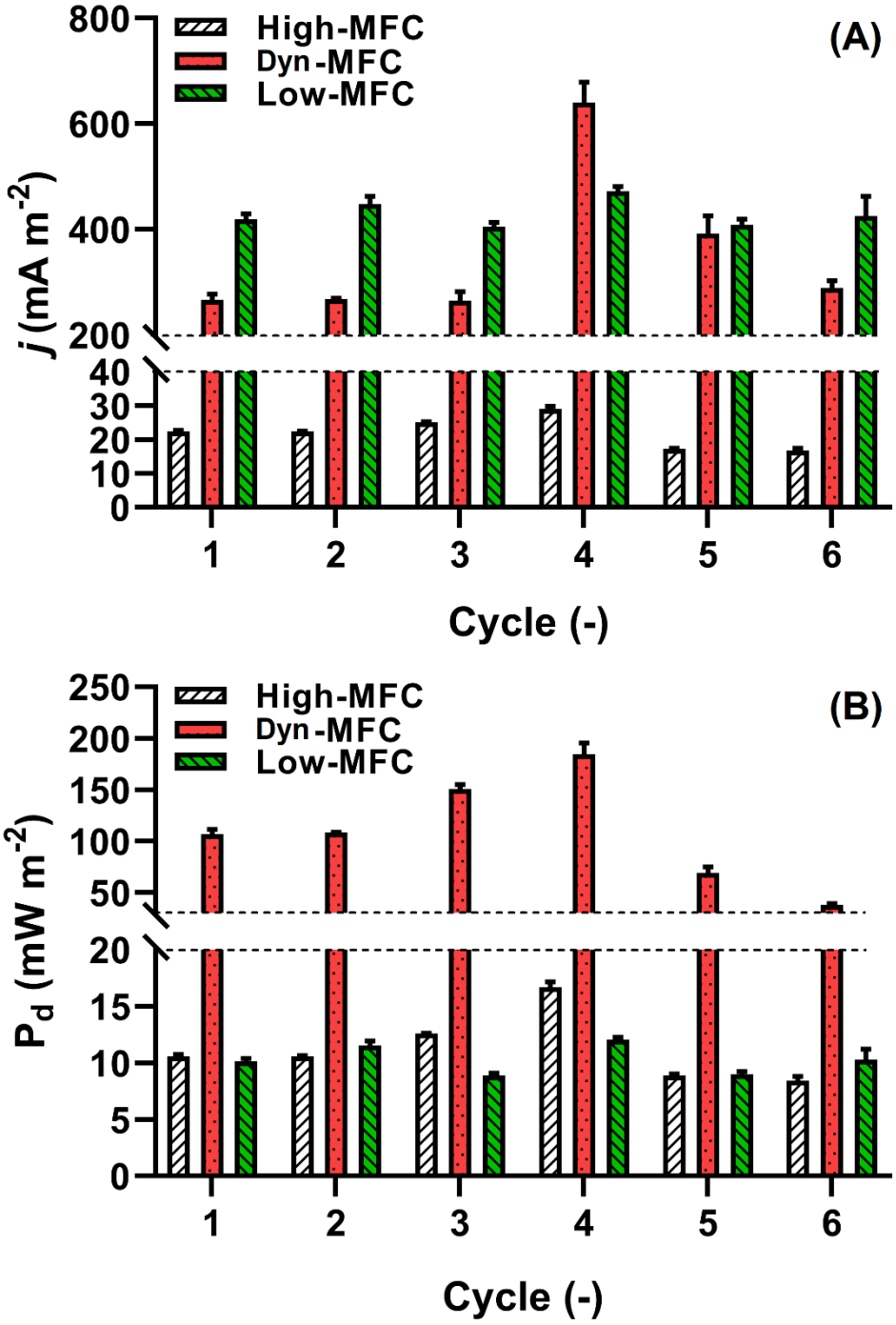

791

792

793 **Fig. 3**

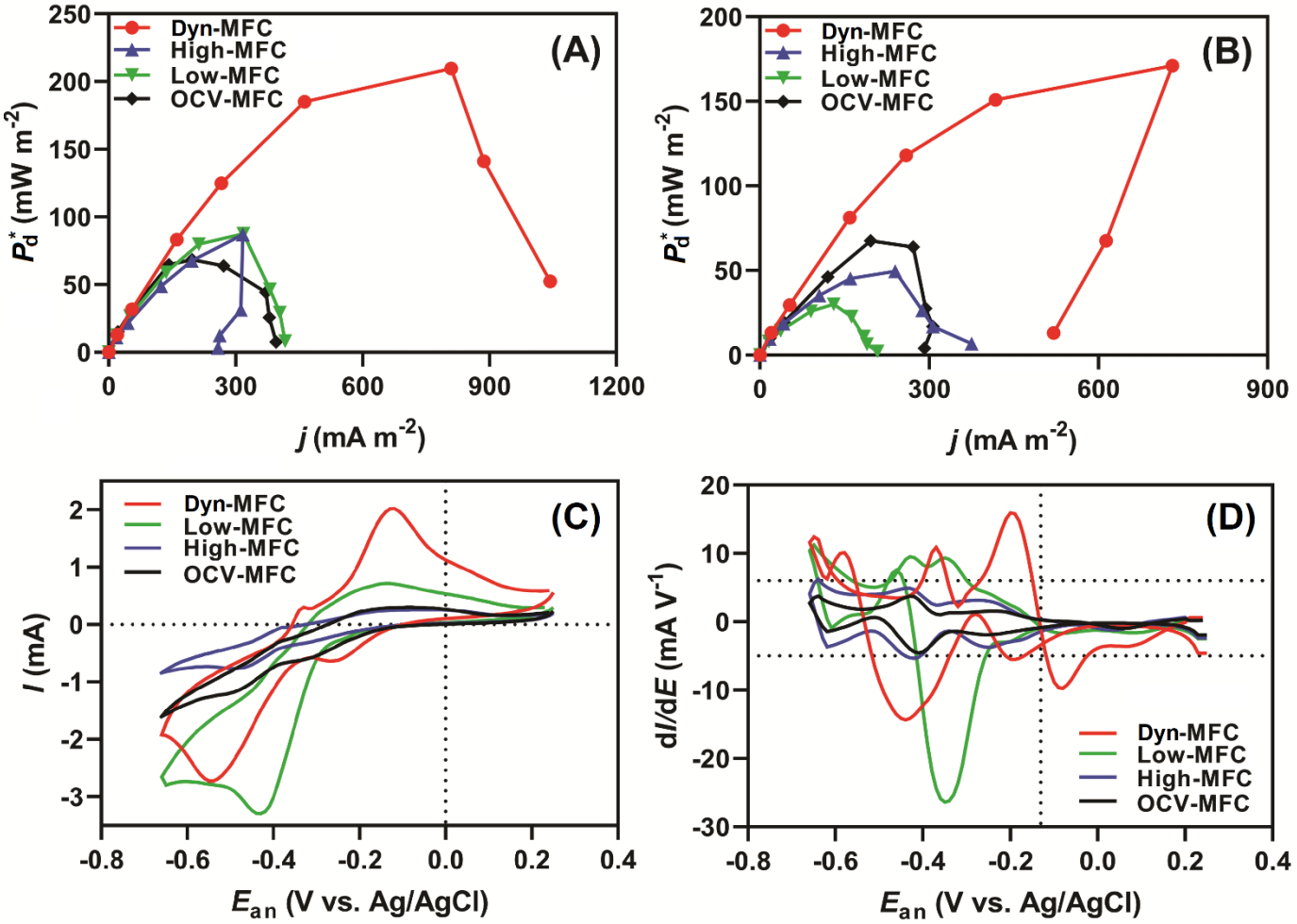

794

795

796 **Fig. 4**

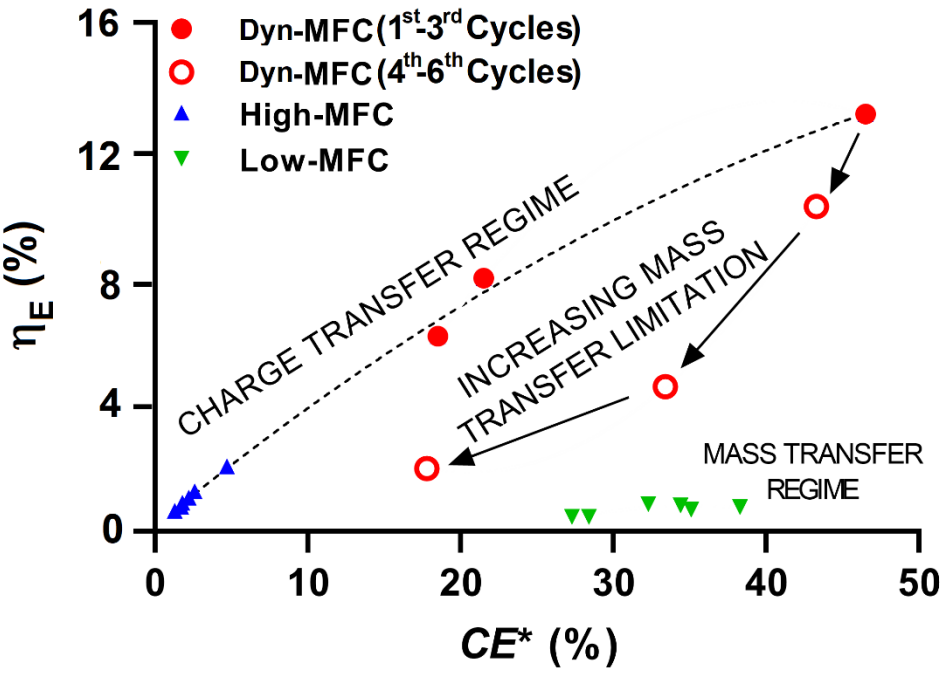

797

798

799

800 **Fig. 5**

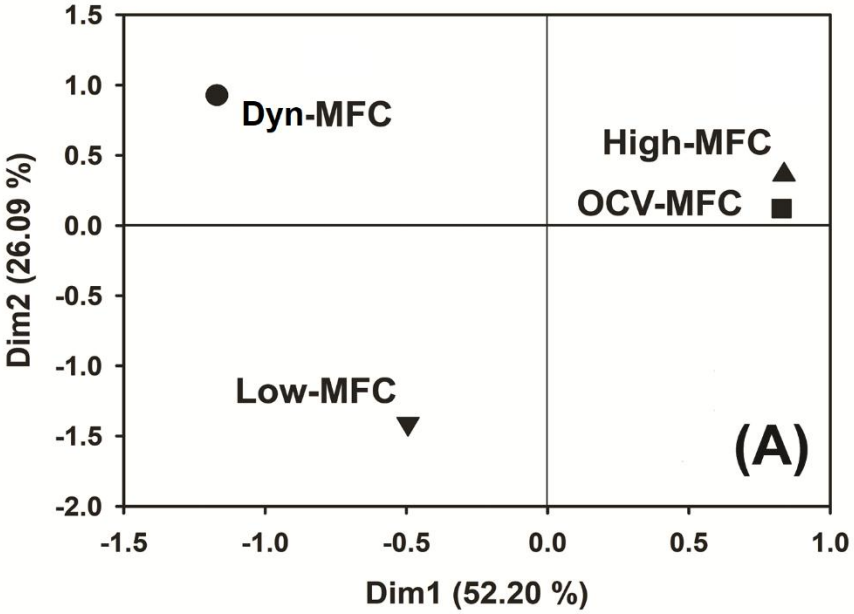

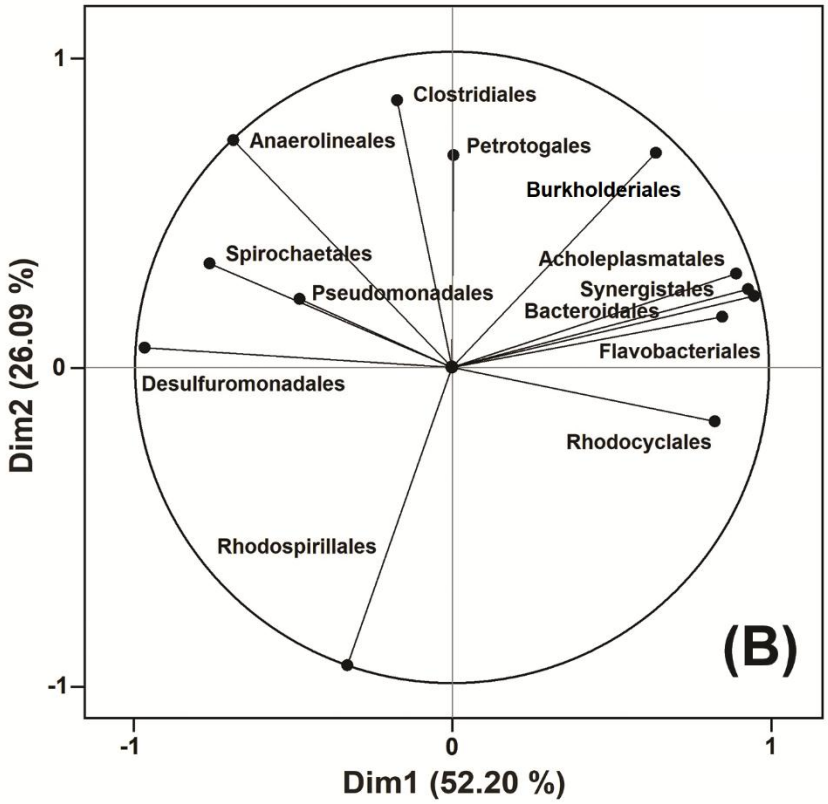

801

802

803 **Fig. 6**

804

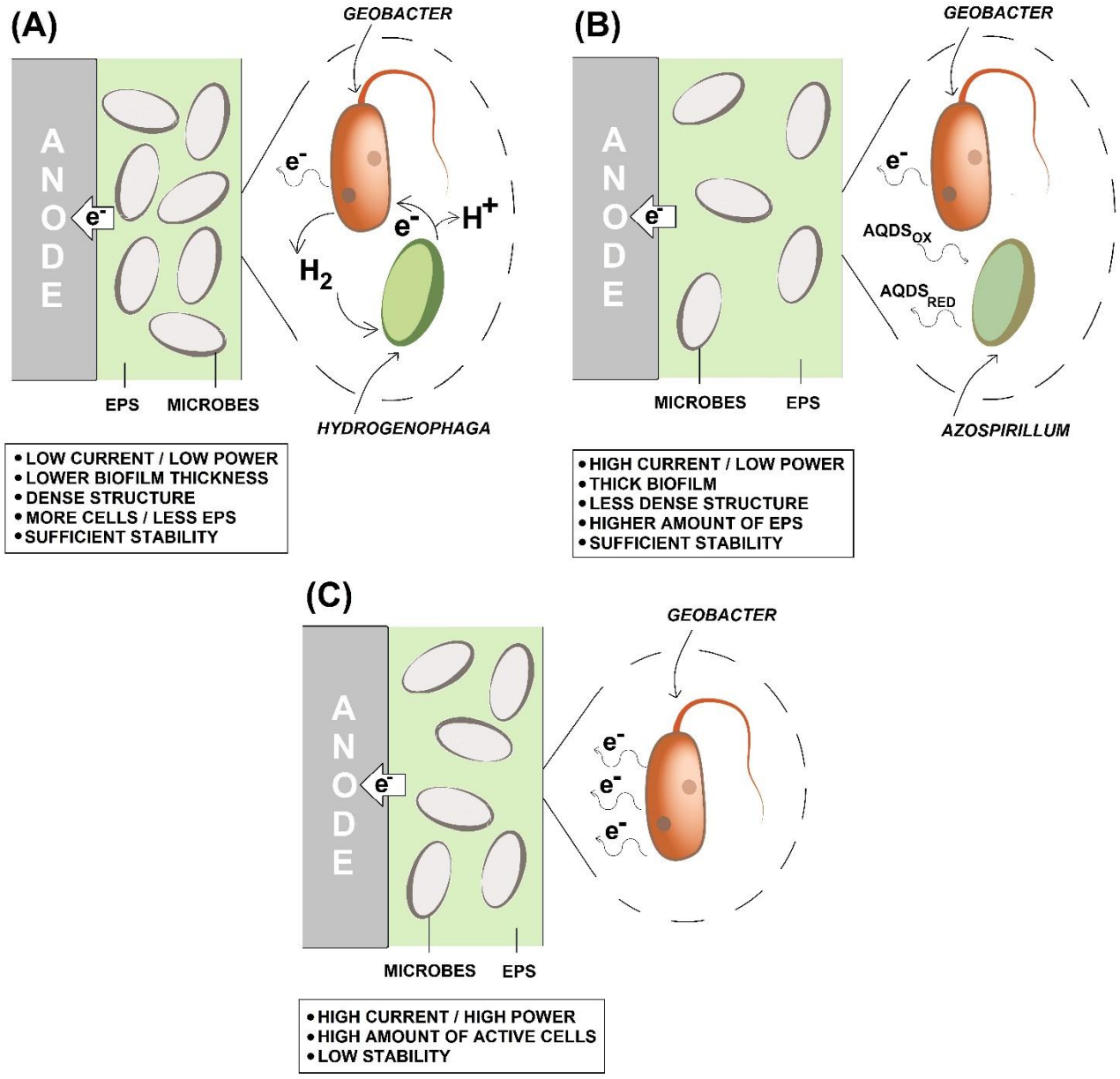

805